PHYSICAL REVIEW B64, 184509 (2001)

Ground State of the Three-Band Hubbard Model

Takashi Yanagisawa, Soh Koike and Kunihiko Yamaji
Condensed-Matter Physics Group, Nanoelectronics Research Institute (NeRI), National Institute of Advanced Industrial Science and Technology (AIST), Central 2 1-1-1 Umezono, Tsukuba, Ibaraki 305-8568, Japan

(18 October 2001)

The ground state of the two-dimensional three-band Hubbard model in the oxide superconductors is investigated by using the variational Monte Carlo method. The Gutzwiller-projected BCS and SDW wave functions are employed in search for a possible ground state with respect to dependences on electron density. Antiferromagnetic correlations are considerably strong near half-filling. It is shown that the d-wave state may exist away from half-filling for both the hole and electron doping cases. Overall structure of the phase diagram obtained by our calculations qualitatively agrees with experimental indications. The superconducting condensation energy is in reasonable agreement with the experimental value obtained from specific heat and critical magnetic field measurements for optimally doped samples. The inhomogeneous SDW state is also examined near 1/8 doping. Incommensurate magnetic structures become stable due to hole doping in the underdoped region, where the transfer t_{pp} between oxygen orbitals plays an important role in determining a stable stripe structure.

PACS numbers: 74.20.-z,74.25.Dw,71.10.Fd.

I. Introduction

In order to investigate the mechanism of superconductivity (SC) in cuprate high-T_c superconductors,[1] we examine the ground state of the two-dimensional three-band Hubbard model for CuO_2 planes which are contained usually in their crystal structures. It is believed that the CuO_2 plane contains the essential features of high-T_c cuprates.[2,3] It is not an easy task to clarify the ground state properties of the 2D three-band Hubbard model because of strong correlations among d and p electrons. We must treat the strong correlations properly to understand the phase diagram of the high-T_c cuprates. The quantum variational Monte Carlo method (VMC) is a tool to investigate the overall structure of phase diagram from weak to strong correlation regions. In this paper we investigate possible ground states in the three-band Hubbard model for CuO_2 plane by employing VMC.

Superconductivity in the one-band Hubbard model has been studied by numerical[4–13] and analytical[14–19] calculations. The three-band Hubbard model has also been investigated with intensive efforts recently.[20–29] The exact diagonalization computations for the three-band model in early stage of high-T_c research supported a possibility of superconductivity by showing that holes can bind in small systems.[30,31] It is also reported that the attractive interaction works for both the d-wave and extended-s wave channels based on finite temperature quantum Monte Carlo (QMC) simulations.[21] It has been shown recently that one can predict finite T_c for the three-band Hubbard model based on perturbative calculations such as generalized RPA treatments.[26–28] In perturbative treatments of the one-band and three-band Hubbard models, the spin fluctuations induced by the on-site Coulomb interaction promote anisotropic pairing correlations. QMC evaluations with some constraints due to the fermion sign problem are against a possibility of superconductivity in the three-band Hubbard model.[25]

In order to investigate the possibility and origin of superconductivity, the recent work by Kondo is important where it has been shown that the d-wave state has lower energy than the normal state for small U by employing the perturbation theory in U for the one-band Hubbard model.[32] This indicates that the ground state is superconductive with d-wave symmetry for small values of U. We can expect that this also holds for the three-band model.[33] It is then natural to expect that the d-wave state is stable for finite U unless there occurs some ordering in the ground state. Among several possible long-range orderings, antiferromagnetic one should be examined because the state with antiferromagnetic ordering is considerably stable near half-filling. In fact, according to VMC work for the one-band Hubbard model, the antiferromagnetic (AF) energy gain is larger than the SC energy gain by almost two order of magnitude near half-filling. Then the competition between SC and AF states is very severe for the SC state.[12,13] The SC region for the one-band Hubbard model is considerably restricted and a possibility of pure superconducting state is very small.[12] A similar feature has been obtained by VMC evaluations for $U_d = \infty$ three-band Hubbard model[34] where antiferro-

magnetic region extends up to 50 percent doping and the d-wave phase exists only in the infinitesimally small region near the boundary of antiferromagnetic phase. Thus VMC results performed recently are consistent with the constrained path QMC calculations[25] in the sense that a possibility of d-wave phase for the one-band Hubbard model and $U_d = \infty$ three-band Hubbard model is small at present, although an attractive interaction works for d-wave pairing.

We expect that the antiferromagnetic region will shrink for the three-band Hubbard model if we adjust parameters contained in the model. The parameters of the three-band Hubbard model are given by the Coulomb repulsion U_d, energy levels of p electrons ϵ_p and d electron ϵ_d, and transfer between p orbitals given by t_{pp}. A purpose of this paper is to investigate the property of antiferromagnetic state and a competition between antiferromagnetism and superconductivity for finite U_d based on the three-band model following ansatz of Gutzwiller-projected wave functions.

It has also been argued that holes doped in the antiferromagnetically correlated spin systems induce incommensurate spin correlations in the ground state for the one-band Hubbard model[35–40] and three-band model[41] within the mean field approximation. In the mean-field treatment the energy scales appear to be extremely large compared to values for real materials. Recent neutron-scattering experiments revealed incommensurate spin structures[42–49] developed at low temperatures and at low energies. The static incommensurate structure was reported on LSCO samples: $La_{2-x}Sr_xCuO_4$, $La_{1.6-x}Nd_{0.4}CuO_4$ and $La_{2-x}Sr_xNiO_{4+y}$. The incommensurate magnetic peaks have been also reported for $YBa_2Cu_3O_{7-\delta}$ by the inelastic neutron-scattering experiments. This type of inhomogeneous state may possibly provide a key concept to resolve the anomalous properties of high-T_c cuprates in the underdoped region. We will examine a possible phase of incommensurate states for the three-band Hubbard model by variational Monte Carlo method.

The paper is organized as follows. In the next section the wave functions are presented. The SC state and uniform SDW state are discussed in Section III and a stability of incommensurate state is examined in the subsequent section. A summary is given in the last section.

II. Hamiltonian and Wave Functions

The Hamiltonian is given as[25,34,50]

$$\begin{aligned} H &= \epsilon_d \sum_{i\sigma} d^\dagger_{i\sigma} d_{i\sigma} + \epsilon_p \sum_{i\sigma} (p^\dagger_{i+\hat{x}/2,\sigma} p_{i+\hat{x}/2,\sigma} + p^\dagger_{i+\hat{y}/2,\sigma} p_{i+\hat{y}/2,\sigma}) \\ &+ t_{dp} \sum_{i\sigma} [d^\dagger_{i\sigma} (p_{i+\hat{x}/2,\sigma} + p_{i+\hat{y}/2,\sigma} - p_{i-\hat{x}/2,\sigma} - p_{i-\hat{y}/2,\sigma}) + h.c.] \\ &+ t_{pp} \sum_{i\sigma} [p^\dagger_{i+\hat{y}/2,\sigma} p_{i+\hat{x}/2,\sigma} - p^\dagger_{i+\hat{y}/2,\sigma} p_{i-\hat{x}/2,\sigma} - p^\dagger_{i-\hat{y}/2,\sigma} p_{i+\hat{x}/2,\sigma} + p^\dagger_{i-\hat{y}/2,\sigma} p_{i-\hat{x}/2,\sigma} + h.c.] \\ &+ U_d \sum_i d^\dagger_{i\uparrow} d_{i\uparrow} d^\dagger_{i\downarrow} d_{i\downarrow} \\ &= H_0 + V, \end{aligned} \tag{1}$$

where

$$V = U_d \sum_i d^\dagger_{i\uparrow} d_{i\uparrow} d^\dagger_{i\downarrow} d_{i\downarrow}. \tag{2}$$

$\hat{x}$ and $\hat{y}$ represent unit vectors along x and y directions, respectively. $p^\dagger_{i\pm\hat{x}/2,\sigma}$ and $p_{i\pm\hat{x}/2,\sigma}$ denote the operators for the p electrons at site $R_i \pm \hat{x}/2$. Similarly $p^\dagger_{i\pm\hat{y}/2,\sigma}$ and $p_{i\pm\hat{y}/2,\sigma}$ are defined. Other notations are standard and energies are measured in units of t_{dp}. For simplicity we neglect the Coulomb interaction among p electrons.

We consider the normal state, BCS and SDW wave functions with the Gutzwiller projection. These types of functions are standard wave functions and well describe the ground-state properties with several long-range orderings. They have been investigated intensively for the one-band Hubbard model.[11–13,51–55] In Refs.[51,55] it has been discussed that they can be improved systematically by operating correlation factors $e^{-\lambda H_0} e^{-\alpha V}$. For the model shown above they are written as

$$\psi_n = P_G \prod_{|k|\le k_F,\sigma} \alpha^\dagger_{k\sigma} |0\rangle, \tag{3}$$

$$\psi_{SC} = P_G P_{N_e} \prod_k (u_k + v_k \alpha^\dagger_{k\uparrow} \alpha^\dagger_{-k\downarrow}) |0\rangle, \tag{4}$$

$$\psi_{SDW} = P_G \prod_{|k|\le k_F,\sigma} \beta^\dagger_{k\sigma} |0\rangle, \tag{5}$$

where $\alpha_{k\sigma}$ is the linear combination of $d_{k\sigma}$, $p_{xk\sigma}$ and $p_{yk\sigma}$ constructed to express an operator for the lowest band of a non-interacting Hamiltonian in the hole picture. For $t_{pp} = 0$, $\alpha_{k\sigma}$ is expressed in terms of a variational parameter $\tilde{\epsilon_p} - \tilde{\epsilon_d}$:

$$\alpha^{\dagger}_{k\sigma} = \left[\frac{1}{2}\left(1+\frac{\tilde{\epsilon_p}-\tilde{\epsilon_d}}{2E_k}\right)\right]^{1/2} d^{\dagger}_{k\sigma} + \mathrm{i}\left[\frac{1}{2}\left(1-\frac{\tilde{\epsilon_p}-\tilde{\epsilon_d}}{2E_k}\right)\right]^{1/2}\left(\frac{w_{xk}}{w_k}p^{\dagger}_{xk\sigma}+\frac{w_{yk}}{w_k}p^{\dagger}_{yk\sigma}\right), \tag{6}$$

where $w_{xk} = 2t_{dp}\sin(k_x/2)$, $w_{yk} = 2t_{dp}\sin(k_y/2)$, $w_k = (w_{xk}^2 + w_{yk}^2)^{1/2}$ and $E_k = [(\tilde{\epsilon_p}-\tilde{\epsilon_d})^2/4 + w_k^2]^{1/2}$. The Fourier transforms of d- and p- electron operators are defined as

$$d^{\dagger}_{k\sigma} = \frac{1}{N^{1/2}}\sum_i d^{\dagger}_{i\sigma}\mathrm{e}^{\mathrm{i}k\cdot R_i}, \tag{7}$$

$$p^{\dagger}_{xk\sigma} = \frac{1}{N^{1/2}}\sum_i p^{\dagger}_{i+\hat{x}/2\sigma}\mathrm{e}^{\mathrm{i}k\cdot(R_i+\hat{x}/2)}, \tag{8}$$

$$p^{\dagger}_{yk\sigma} = \frac{1}{N^{1/2}}\sum_i p^{\dagger}_{i+\hat{y}/2\sigma}\mathrm{e}^{\mathrm{i}k\cdot(R_i+\hat{y}/2)}, \tag{9}$$

where N is the total number of cells which consist of d, p_x and p_y orbitals. Coefficients u_k and v_k, appearing only as a ratio, are given by the BCS form:

$$\frac{v_k}{u_k} = \frac{\Delta_k}{\xi_k + (\xi_k^2+\Delta_k^2)^{1/2}}, \tag{10}$$

for $\xi_k = \epsilon_k - \mu$ where ϵ_k is the energy dispersion for the lowest band. P_G is the Gutzwiller projection operator for the Cu d site and P_{N_e} is a projection operator which extracts only the states with a fixed total electron number. The SC order parameter Δ_k is assumed to have the following $d_{x^2-y^2}$- and extended s-wave form:

$$\mathrm{d} \quad \Delta_k = \Delta_s(\cos k_x - \cos k_y), \tag{11}$$

$$\mathrm{s}^* \quad \Delta_k = \Delta_s(\cos k_x + \cos k_y). \tag{12}$$

Equation (4) is written as

$$\psi_{SC} = P_G\left(\sum_k \frac{v_k}{u_k}\alpha^{\dagger}_{k\uparrow}\alpha^{\dagger}_{-k\downarrow}\right)^{N_e/2}. \tag{13}$$

The wave function given by eq.(13) agrees with

$$\psi_{BCS} = P_G\prod_k(u_k + v_k\alpha^{\dagger}_{k\uparrow}\alpha^{\dagger}_{-k\downarrow})|0\rangle, \tag{14}$$

in the thermodynamic limit. For the commensurate SDW state $\beta_{k\sigma}$ is given by a linear combination of two wave numbers $\mathbf{k}$ and $\mathbf{k}+\mathbf{Q}$ for the commensurate vector $\mathbf{Q} = (\pi,\pi)$. We can also investigate the incommensurate SDW state with incommensurate vector $\mathbf{Q} = (\pi \pm 2\pi\delta, \pi)$ by diagonalizing the Hartree-Fock Hamiltonian with antiferromagnetic long-range order. The system sizes are given by 6×6 and 8×8 for the projected BCS wave function and 16×4, 24×6, 32×8, 40×10 and 16×16 for the incommensurate SDW states. Our calculations are performed with the periodic and the antiperiodic boundary conditions for the x- and y-direction, respectively. This set of boundary conditions was chosen so that Δ_k does not vanish for any $\mathbf{k}$-points possibly occupied by electrons.

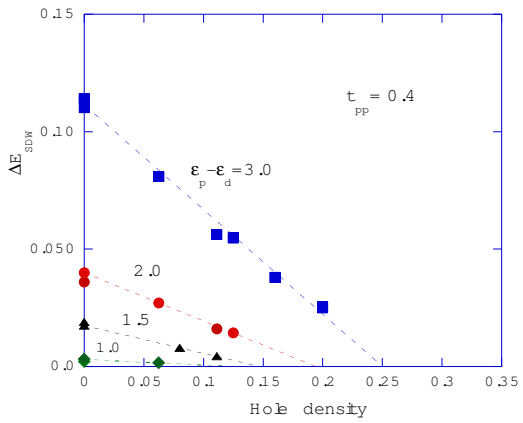

FIG. 1. Energy per site $(E_{normal} - E)/N$ of the SDW state as a function of hole density δ for $t_{pp} = 0.4$ and $U_d = 8$. From the top, $\epsilon_p - \epsilon_d = 3$, 2, 1.5 and 1. The results are for 6×6, 8×8, 10×10 and 16×12 systems. Antiperiodic and periodic boundary conditions are imposed in x- and y-direction, respectively. Monte Carlo statistical errors are smaller than the size of symbols. Curves are guide for eyes.

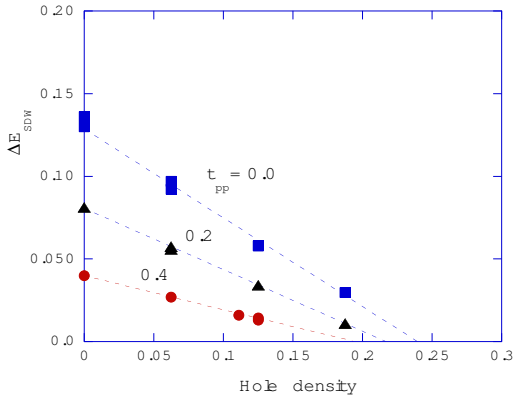

FIG. 2. Energy per site $(E_{normal} - E)/N$ of the SDW state as a function of hole density δ for $t_{pp} = 0.0$, 0.2 and 0.4 where $\epsilon_p - \epsilon_d = 2$ and $U_d = 8$. The results are for 6×6, 8×8, 10×10 and 16×12 systems. Curves are guide for eyes.

The expectation values are calculated following the standard Monte Carlo procedure by using the Metropolis algorithm. In the process of finding a minimum of energy, we should optimize many parameters included in the wave functions. For such purpose we employ correlated measurements method to reduce the required cpu time.[56]

III. Condensation energy and phase diagram

First, let us discuss the SDW phase near half-filling by evaluating the ground-state energy for optimized parameters g, $\tilde{\epsilon_p} - \tilde{\epsilon_d}$ and AF order parameter Δ_{AF}. We

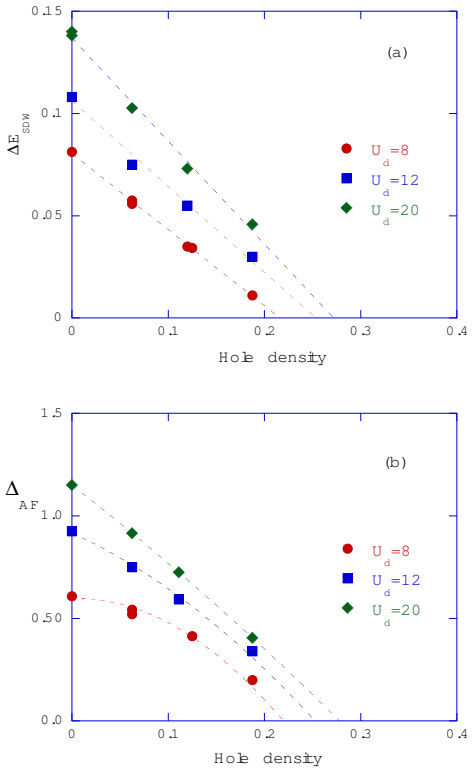

FIG. 3. (a) Energy per site $(E_{normal} - E)/N$ of the SDW state as a function of hole density δ for $U_d = 8$, 12 and 20 where $\epsilon_p - \epsilon_d = 2$ and $t_{pp} = 0.2$. (b) Antiferromagnetic order parameter as a function of hole density for $U_d = 8$, 12 and 20 where $\epsilon_p - \epsilon_d = 2$ and $t_{pp} = 0.2$. The results are for 6×6, 8×8, 10×10 and 16×12 systems. Curves are guide for eyes.

set $\epsilon_p = 0$ throughout this paper. It is expected that holes introduced by doping are responsible for the disappearance of long-range antiferromagnetic ordering.[57–59] We show the SDW energy gain ΔE_{SDW} in Fig.1 as a function of doping ratio for several values of $\epsilon_p - \epsilon_d$. ΔE_{SDW} increases and the SDW region becomes large as $\epsilon_p - \epsilon_d$ increases. The figure 2 shows the SDW energy gain for several values of t_{pp}, where ΔE_{SDW} is reduced as t_{pp} increases. In Figs.3(a) and 3(b) the dependence on Coulomb repulsion U_d is shown; the SDW phase extends up to 30 percent doping when U_d is large. Then it follows that the SDW region will be reduced if $\epsilon_p - \epsilon_d$ and U_d decrease or t_{pp} increases. In fact, Fig.4 shows the boundary of SDW phase in the t_{pp}-δ plane for $U_d = 8$ where δ is the hole density and negative density indicates electron doping. Compared to the calculations for $U_d = \infty$ the SDW region is reduced greatly.[34]

Next, let us turn to the projected-BCS wave function, where the Gutzwiller parameter g, effective level difference $\tilde{\epsilon_p} - \tilde{\epsilon_d}$, chemical potential μ and superconducting order parameter Δ_s are considered as variational parameters. In Fig.5 we show the energy as a function of Δ_s where $t_{pp} = 0.0$, $U_d = 8$ and $\epsilon_p - \epsilon_d = 2$ and doping ratio is given by $\delta = 0.111$ for (a) and $\delta = 0.333$ for (b). The d-wave superconductivity is most stable among various

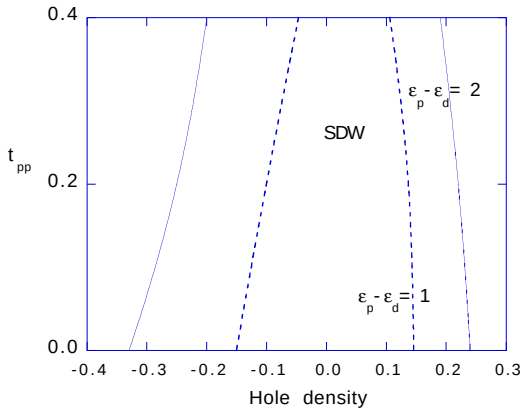

FIG. 4. Boundary of the SDW state in the plane of t_{pp}-δ for $\epsilon_p - \epsilon_d = 2$ and 1. We set $U_d = 8$.

possible states such as isotropic s-wave and anisotropic s-wave pairing states. The squares in Fig.5 denote the values for the normal state, which are estimated independently by using an alternative Monte Carlo algorithm. The finite SC energy gain indicates that the attractive interaction works for d-wave pairing.

The SC energy gain (which is called the SC condensation energy in this paper) is also dependent on $\epsilon_p - \epsilon_d$, as is shown in Fig.6 for $t_{pp} = 0.2$, $U_d = 8$ and $\delta = 0.111$ on 6×6 lattice. This shows a tendency that the SC condensation energy increases as $\epsilon_p - \epsilon_d$ increases, which is consistent with calculations for $U_d = \infty$.[34] It is noted that the dependence on $\epsilon_p - \epsilon_d$ for the SC energy gain is rather weak compared to the SDW energy gain. We also note that the SC energy gains for $U_d = 8$ are mostly of the same order of those for $U_d = \infty$.[34]

From the calculations for the SDW wave functions, we should set $\epsilon_p - \epsilon_d$ and U_d small so that the SDW phase does not occupy a huge region near half-filling. In Fig.7 we show energy gains for both the SDW and SC states for $U_d = 8$, $t_{pp} = 0.2$ and $\epsilon_p - \epsilon_d = 2$, where the negative delta indicates the electron-doping case. Solid symbols indicate the results for 8×8 and open symbols for 6×6. For this set of parameters the SDW region extends up to 20 percent doping and the pure d-wave phase exists outside of the SDW phase. The d-wave phase may be possibly identified with superconducting phase in the overdoped region in the high-T_c superconductors.

The superconducting condensation energy obtained by our calculations is estimated as $E_{cond} \simeq 0.0005 t_{dp} = 0.75$meV per site in the overdoped region near the boundary of SDW phase from the difference between the minimum and the intercept of the $E/N - \Delta_s$ curve with the vertical axis, where we set $t_{dp} = 1.5$eV as estimated from cluster calculations.[60–62] We have also estimated E_{cond} from several experiments such as specific heat or critical field measurements for optimally doped samples. They are given as $0.17 \simeq 0.26$meV from specific heat data[12,63,64] and 0.26meV from critical magnetic field value $H_c^2/8\pi$.[12,65] Our value is in reasonable agreement with the experimental data as was already shown for the

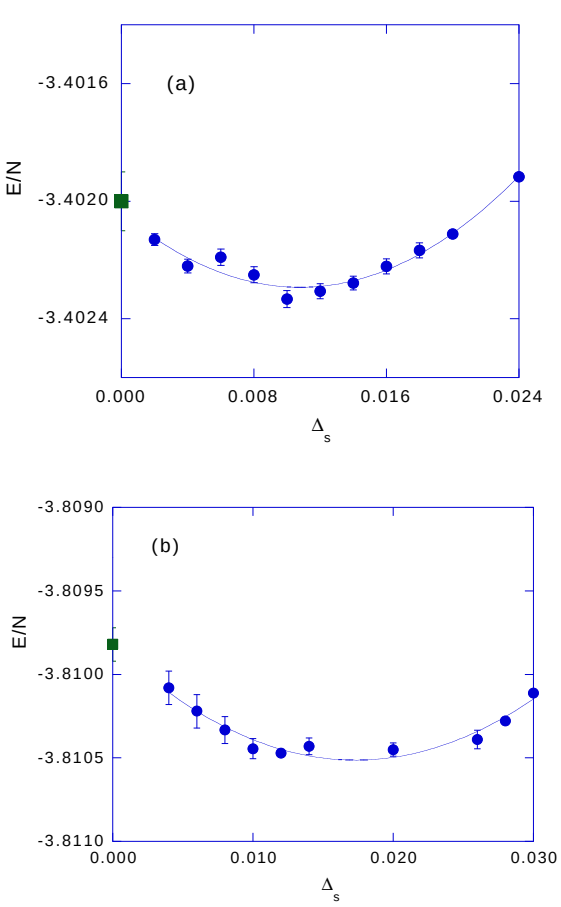

FIG. 5. Ground state energy per site as a function of Δ_s on 6×6 lattice for (a) $\delta = 0.111$ and $t_{pp} = 0.0$, and (b) $\delta = 0.333$ and $t_{pp} = 0.0$. Parameters are given by $U_d = 8$ and $\epsilon_p - \epsilon_d = 2$ in units of t_{dp}. Squares denote the energies for the normal state evaluated independently.

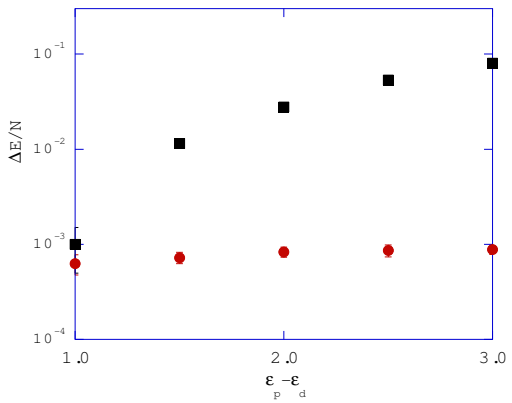

FIG. 6. Superconducting (circles) and antiferromagnetic (squares) energy gains per site as a function of $\epsilon_p - \epsilon_d$ for $t_{pp} = 0.2$ and $U_d = 8$ on 6×6 lattice.

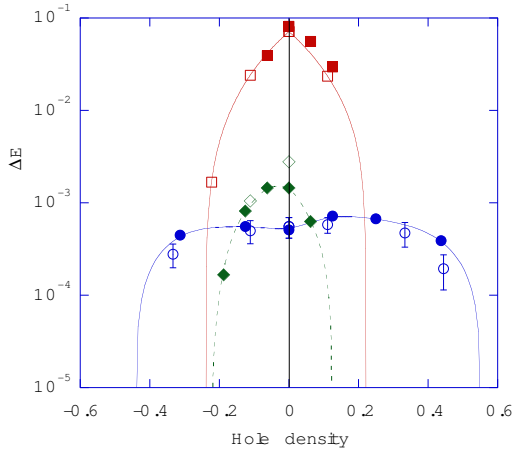

FIG. 7. Condensation energy per site as a function of hole density δ for $t_{pp} = 0.2$, $\epsilon_p - \epsilon_d = 2$ and $U_d = 8$. Circles, squares and diamonds denote the energy gain per site in reference to the normal state energy for d-wave, SDW and extended-s wave states, respectively. Solid symbols are for 8×8 and open symbols are for 6×6. Curves are guide for eyes.

Hubbard model where the SC energy gain in the bulk limit is given by 0.00117t/site=0.59meV/site.[54] This agreement between the theoretical and experimental condensation energy is highly remarkable. We expect that this value is not far from the correct value according to the evaluations for improved wave functions,[51] where it was shown that the energy gain is not changed so much due to multiplicative correlation factors $e^{-\Delta\tau H_0} e^{-\Delta\tau V}$. We cannot estimate the SC condensation energy in the underdoped region because the SDW state is more stable than d-wave state and the SC condensation energy is not available experimentally due to a loss of entropy in the underdoped region.[63]

The phase structure obtained by our calculations agrees well with the available phase diagram indicated by experiments qualitatively, which means that a large SDW phase exists in the underdoped region and there is a d-wave superconducting phase next to SDW phase in the overdoped region. Our calculations for electron-doping case predict d-wave symmetry away from half-filling, which is consistent with recent experiments on $Nd_{1.85}Ce_{0.15}CuO_{4-y}$.[66]

IV. Incommensurate antiferromagnetism with spin modulation

In this section let us discuss the underdoped region where the SDW state is significantly stable as shown in the previous section. Let us note that the SDW state can be possibly stabilized further if we take into account a spin modulation in space, as has also been studied for the one-band Hubbard model[35–40,67] and the t-J model.[68–71] We can introduce a stripe in the uniform spin density state so that doped holes occupy new levels close to the starting Fermi energy keeping the energy loss of antiferromagnetic background minimum. The wave func-

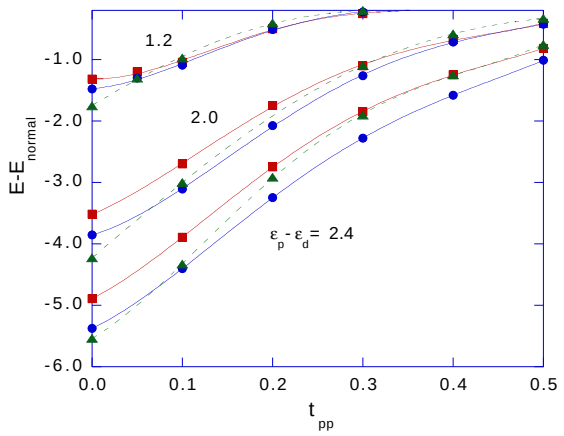

FIG. 8. Energies of commensurate and incommensurate SDW states on 16×4 lattice at $\delta = 1/8$ for $U_d = 8$. Circles and triangles are for 4-lattice and 8-lattice stripes, respectively. Squares denote energy for commensurate SDW state. From the top $\epsilon_p - \epsilon_d = 1.2$, 2.0 and 2.4. We impose antiperiodic boundary condition in x-direction and periodic boundary condition in y-direction. Monte Carlo statistical errors are within the size of symbols.

tion with a stripe can be taken of the Gutzwiller type: $\psi_{stripe} = P_G \psi^0_{stripe}$. ψ^0_{stripe} is the Slater determinant made from solutions of the Hartree-Fock Hamiltonian[67]

$$H_{stripe} = H^0_{dp} + \frac{U}{2} \sum_{i\sigma} [\langle n_{di} \rangle - \sigma(-1)^{x_i+y_i} \langle m_i \rangle] d^\dagger_{i\sigma} d_{i\sigma}, \quad (15)$$

where H^0_{dp} is the non-interacting part of the Hamiltonian H with variational parameter $\tilde{\epsilon_p} - \tilde{\epsilon_d}$. $\langle n_{di} \rangle$ and $\langle m_i \rangle$ are expressed in terms of modulation vectors Q_s and Q_c for spin and charge part, respectively. Including the constant part of $\langle n_{di} \rangle$ in the definition of variational parameter $\tilde{\epsilon_d}$, we diagonalize the following one-particle Hamiltonian to determine ψ^0_{stripe}:

$$H_{stripe} = H^0_{dp} + \sum_{i\sigma} [\delta n_{di} - \sigma(-1)^{x_i+y_i} m_i] d^\dagger_{i\sigma} d_{i\sigma}. \quad (16)$$

δn_{di} and m_i are assumed to have the form

$$\delta n_{di} = -\sum_j \alpha / \cosh((x_i - x^{str}_j)/\xi_c), \quad (17)$$

$$m_i = m \prod_j \tanh((x_i - x^{str}_j)/\xi_s), \quad (18)$$

with parameters α, m, ξ_c and ξ_s. x^{str}_j denotes the position of a stripe. In actual calculations we set $\xi_c = 1$ and $\xi_s = 1$ since the energy expectation values are mostly independent of ξ_c and ξ_s. Since any eigenfunction of the Hamiltonian H^0_{dp} can be a variational wave function, we optimize α instead of fixing it in order to lower the energy expectation value further. It is also possible to assume that δn_{di} and m_i oscillate according to cosine curve given

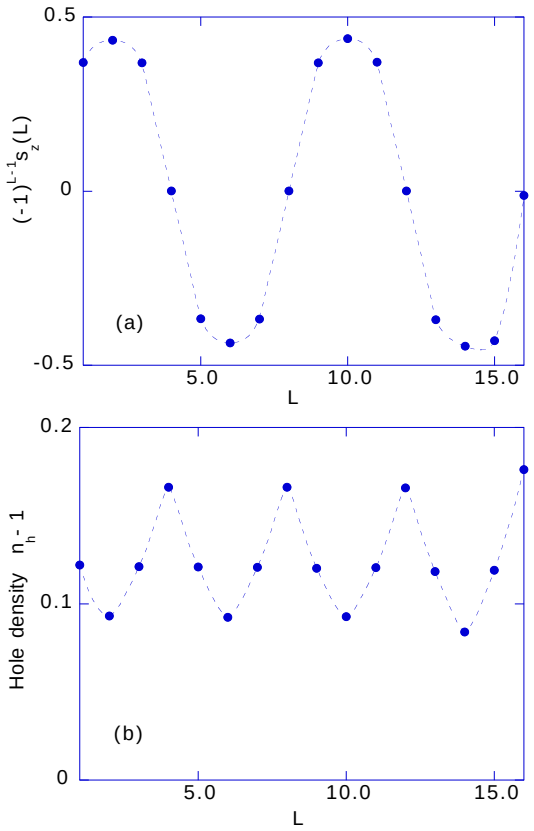

FIG. 9. Spin (a) and charge (b) densities for incommensurate state at $\delta = 1/8$ for $t_{pp} = 0.4$, $U_d = 8$ and $\epsilon_p - \epsilon_d = 2$ on 16×4 lattice. The boundary conditions are same as in Fig.8

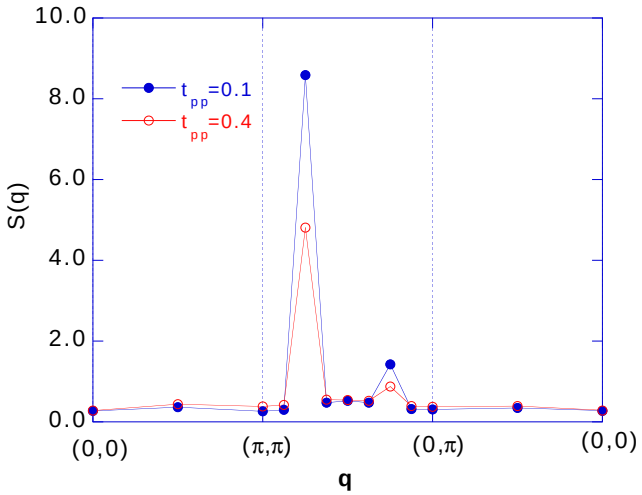

FIG. 10. Spin structure function for incommensurate state at $\delta = 1/8$ for $t_{pp} = 0.4$, 0.1 and $\epsilon_p - \epsilon_d = 2$ on 16×4 lattice. We set $U_d = 8$. The boundary conditions are same as in Fig.8.

as $\cos(4\pi\delta x_i)$ and $\cos(2\pi\delta x_i)$, respectively. Both methods give almost the same results within Monte Carlo statistical errors.

Recent neutron scattering experiments suggested that modulation vectors are given by $Q_s = (\pi \pm 2\pi\delta, \pi)$ and $Q_c = (\pm 4\pi\delta, 0)$ in the underdoped region, where δ denotes the doping ratio. Here we define n-lattice stripe as an incommensurate state with one stripe per n ladders for which Q_s is given by $Q_s = (\pi \pm \pi/n, \pi)$. Then the incommensurate state predicted by neutron experiments for $\delta = 1/8$ is given by 4-lattice stripe. For the three-band model, the transfer t_{pp} between oxygen orbitals plays an important role to determine a possible SDW state. If t_{pp} is very large, the uniform SDW state is expected to be stabilized because holes doped on oxygen sites can move around on the lattice producing disorder effect on spin ordering uniformly. For small t_{pp} the stripe states are considered to be realized.[41] Our motivation to consider non-uniform states for the three-band model lies in the idea that the distance between stripes may be dependent upon t_{pp}, i.e. for small t_{pp} the distance between stripes is large, for intermediate values of t_{pp} the 4-lattice stripe state is realized and for large t_{pp} the uniform state or normal state is stable.

In Fig.8 we show the energies for commensurate and incommensurate SDW states on 16×4 lattice at $\delta = 1/8$ as a function of t_{pp}, where we impose the antiperiodic and periodic boundary conditions in x- and y-direction, respectively, so that the closed shell structure is followed for doped holes. We assumed that $\epsilon_p - \epsilon_d = 1.2$, 2 and 2.4. The 8-lattice stripe state for small t_{pp} changes into uniform state as t_{pp} increases. It shows that incommensurate states become stable for large level difference $\epsilon_p - \epsilon_d$. The spin and charge densities of incommensurate state are shown in Fig.9 for $t_{pp} = 0.4$ and $\epsilon_p - \epsilon_d = 2$ where the charge density is a sum of hole numbers on d-, p_x- and p_y-orbitals at site L. Spin density $S_z(i) = n_{di\uparrow} - n_{di\downarrow}$ vanishes at the positions of stripes associated with peaks of hole density. The spin structure factor $S_z(\mathbf{q})$ really has incommensurate peaks as is shown in Fig.10. The Figures 11(a) and 11(b) present the energies of incommensurate states for 16×16 lattice (which contains 768 atoms) where we set antiperiodic and periodic boundary conditions in x- and y-direction, respectively, for (a) and in y- and x- direction, respectively, for (b). Both figures give almost the same results as an evidence that the effect of boundary conditions is small for 16×16 system. As expected, the structure of incommensurate state is dependent upon the values of t_{pp}.

Let us turn to a discussion of the energy gain due to a formation of stripes, which is estimated from an extrapolation to the bulk limit as shown in Fig.12. One notes that the energy gain increases as the system size increases. The energy gain per site for 4-lattice stripe state is given by $\simeq 0.015 t_{dp} \simeq 22.5$meV. Furthermore the energy difference between commensurate and incommensurate states is found to be finite in the bulk limit, which is shown in Fig.13. Thus within VMC the stripe state with spin modulation is stable at $\delta = 1/8$ doping.

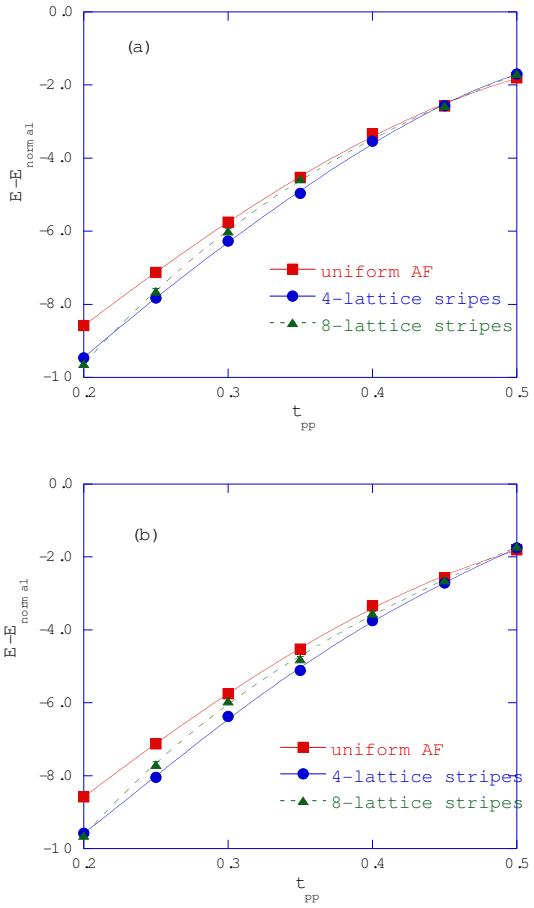

FIG. 11. Energies at $\delta = 1/8$ for 16×16 lattice. Parameters are given by $\epsilon_p - \epsilon_d = 2$, $U_d = 8$ and $t_{pp} = 0.4$. Symbols are the same as in Fig.8. For (a) boundary conditions are antiperiodic and periodic in x- and y-direction, respectively, and for (b) periodic and antiperiodic boundary conditions are imposed in x- and y-direction, respectively. Monte Carlo statistical errors are within the size of symbols.

The antiferromagnetic order parameter m in eq.(18) is of the order of $0.5 t_{dp} \simeq 0.75$eV, while the SC order parameter Δ_s (which gives the minimum of energy) is of the order of $0.01 \sim 0.015 t_{dp} = 15meV\sim$ 20meV at $\delta \sim 0.2$. The magnitude of SC order parameter agrees with measurements of tunneling spectroscopy[72,73] where Δ_s is estimated as $\Delta_s \simeq 17$meV for YBCO sample.[72] The antiferromagnetic order parameter is larger than SC order parameter at least by one order of magnitude. The charge order parameter α in eq.(17) is small and negligible compared to m_i.

V. Summary

We have presented our evaluations for the 2D three-band Hubbard model based on the variational Monte Carlo method. Our work is regarded as a starting step for more sophisticated calculations in future such as the inclusion of correlation factors of Jastrow type or Green function Monte Carlo approaches. The SC energy scales

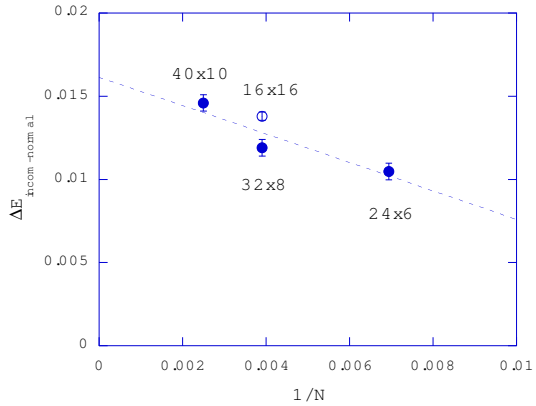

FIG. 12. $E_{normal} - E_{incom}$ as a function of 1/N. Parameters are given by $t_{pp} = 0.4$, $U_d = 8$ and $\epsilon_p - \epsilon_d = 2$. Solid circles are for 24×6, 32×8 and 40×10. Open circle is for 16×16. We set antiperiodic and periodic boundary conditions in x- and y- direction, respectively.

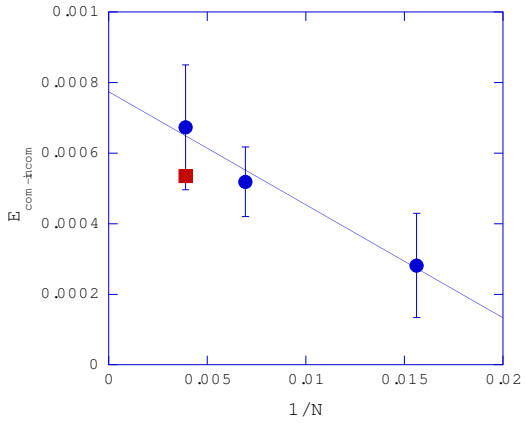

FIG. 13. $E_{com} - E_{incom}$ as a function of 1/N. Parameters are given by $t_{pp} = 0.4$, $U_d = 8$ and $\epsilon_p - \epsilon_d = 2$. Circles are for rectangular lattices and the square is for 16×16. Boundary conditions are the same as in Fig.12

obtained from our evaluations are consistent with experimental indications, which provides a support to our approaches.

According to VMC the attractive interaction works for d-wave pairing due to electron correlations. The strength of U_d is also important to determine the phase boundary of the SDW phase. If U_d is extremely large, the SDW region extends up to large doping for which the d-wave region is restricted to infinitesimally small region near the boundary of antiferromagnetic phase. For intermediate values of U_d and $\epsilon_p - \epsilon_d$ the SDW region is reduced and the d-wave superconducting phase may exist. The fact that the SC condensation energy agrees reasonably with the experimental data for optimally doped samples supports our computations. The magnitude of SC order parameter is also consistent with tunneling spectroscopy experiments. From our data for ΔE_{SC} and Δ_s and the relation $N(0)\Delta_s^2/2 = \Delta E_{SC}$, the effective density of state $N(0)$ can be estimated as $N(0) \simeq 3 \sim 6.7(\mathrm{eV})^{-1} \simeq 4.4 \sim 10/t_{dp}$ at $\delta \sim 0.2$ in the overdoped region, which is not far from the BCS estimate $N(0) \sim 2$ to $3(\mathrm{eV})^{-1}$ by using $N(0)(k_B T_c)^2/2$ for optimally doped YBCO.[64] We expect that the pure d-wave state from optimal to overdoped regions may be described by the projected-BCS wave function. The phase diagram for electron-doping is consistent with the available experimental indications suggesting that the properties of electron-doped materials may be understood within our approach. In the SDW region the incommensurate spin structures are stabilized for the low-doping case to keep the energy loss minimum due to disorder effect caused by holes. A competition among the uniform SDW state, SDW state with stripes, and pure d-wave SC is highly non-trivial. A picture for the hole-doping case followed from our evaluations is that a stripe state is stable in the underdoped region and changes into the d-wave SC in the overdoped region.

We thank S. Koikegami for valuable discussions. The computations were carried out on the alpha cluster machines supported by the ACT-JST program of Japan Science and Technology Cooperation, and also on the HItachi SR8000 at the Tsukuba Advanced Computing Center of the National Institute of Advanced Industrial Science and Technology.

[1] See, for example, *Proceedings of 22nd International Conference on Low Temperature Physics* (LT22) (Helsinki, Finland, 1999) Physica B**284-288** (2000).

[2] V.J. Emery, Phys. Rev. Lett. **58**, 2794 (1987).

[3] L.H. Tjeng, H. Eskes, and G.A. Sawatzky, *Strong Correlation and Superconductivity* edited by H. Fukuyama, S. Maekawa and A.P. Malozemoff (Springer, Berlin Heidelberg, 1989), pp.33.

[4] J.E. Hirsch, Phys. Rev. Lett. **54**, 1317 (1985).

[5] S.R. White, D.J. Scalapino, R.L. Sugar, E.Y. Loh, J.E. Gubernatis, and R.T. Scalettar, Phys. Rev. B**40**, 506 (1989).

[6] N. Furukawa and M. Imada: J. Phys. Soc. Jpn. **61**, 3331 (1992).

[7] E. Dagotto, Rev. Mod. Phys. **66**,763 (1994).

[8] T. Husslein, I. Morgenstein, D.M. Newns, P.C. Pattnaik, J.M. Singer, and H.G. Matuttis, Phys. Rev. B**54**, 16179 (1996).

[9] K. Kuroki, H. Aoki, T. Hotta, and Y. Takada, Phys. Rev. B**55**,2764 (1997).

[10] S. Zhang, J. Carlson, and J.E. Gubernatis, Phys. Rev. Lett. **78**, 4486 (1997).

[11] T. Nakanishi, K. Yamaji and T. Yanagisawa, J. Phys. Soc. Jpn. **66**, 294 (1997).

[12] K. Yamaji, T. Yanagisawa, T. Nakanishi and S. Koike, Physica C **304**, 225 (1998); ibid. 141, (2000).

[13] K. Yamaji, T. Yanagisawa and S. Koike, J. Phys. Chem. Solids **62** 237, (2001); in *Physics in Local Lattice Distortion* edited by A. Bianconi and H. Oyanagi (AIP, New York, 2001), p.222.

[14] D.J. Scalapino, E. Loh, and J.E. Hirsch, Phys. Rev. B**34**, 8190 (1986).

[15] H. Shimahara and S. Takada, J. Phys. Soc. Jpn. **57**, 1044 (1988).

[16] N.E. Bickers, D.J. Scalapino, and S.R. White, Phys. Rev. Lett. **62**, 961 (1989).

[17] C-H. Pao and N.E. Bickers, Phys. Rev. B**49**, 1586 (1994); Phys. Rev. Lett. **72**, 1870 (1994).

[18] P. Monthoux and D.J. Scalapino, Phys. Rev. Lett. **72**, 72 (1994).

[19] T. Dahm and L. Tewordt, Phys. Rev. B**52**, 1297 (1995).

[20] J.E. Hirsch, E.Y. Loh, D.J. Scalapino, and S. Tang, Phys. Rev. B**39**, 243 (1989).

[21] R.T. Scalettar, D.J. Scalapino, R.L. Sugar, and S.R. White, Phys. Rev. B**44**, 770 (1991).

[22] G. Dopf, A. Muramatsu, and W. Hanke, Phys. Rev. B**41**, 9264 (1990).

[23] G. Dopf, A. Muramatsu, and W. Hanke, Phys. Rev. Lett. **68**, 353 (1992).

[24] K. Kuroki and H. Aoki, Phys. Rev. Lett. **76**, 4400 (1996).

[25] M. Guerrero, J.E. Gubernatis and S. Zhang, Phys. Rev.B **57**, 11980 (1998).

[26] T. Hotta, J. Phys. Soc. Jpn. **63**, 4126 (1994).

[27] T. Takimoto and T. Moriya, J. Phys. Soc. Jpn. **66**, 2459 (1997).

[28] A. Kobayashi, A. Tsuruta, T. Matsuura and Y. Kuroda, J. Phys. Soc. Jpn. **67**, 2626 (1998).

[29] S. Koikegami and K. Yamada, J. Phys. Soc. Jpn. **69**, 768 (2000).

[30] M. Ogata and H. Shiba, J. Phys. Soc. Jpn. **57**, 3074 (1988).

[31] W.H. Stephan, W. Linden, and P. Horsch, Phys. Rev. B**39**, 2924 (1989).

[32] J. Kondo, The Bulletin of Electrotechnical Laboratory **64**, 67 (2000); J. Phys. Soc. Jpn. **70**, 808 (2001).

[33] S. Koikegami and T. Yanagisawa, unpublished.

[34] T. Asahata, A. Oguri and S. Maekawa, J. Phys. Soc. Jpn. **65**, 365 (1996).

[35] D. Poilblanc and T.M. Rice, Phys. Rev. B**39**, 9749 (1989).

[36] M. Kato, K. Machida, H. Nakanishi and M. Fujita, J. Phys. Soc. Jpn. **59**, 1047 (1990).

[37] H. Schulz, Phys. Rev. Lett. **64**, 1445 (1990).

[38] J. Zaanen and A.M. Oleś, Ann. Phys. **5**, 224 (1996).

[39] M.I. Salkola, V.J. Emery, and S.A. Kivelson, Phys. Rev. Lett. **77**, 155 (1996).

[40] M. Ichioka and K. Machida, J. Phys. Soc. Jpn. **68**, 4020 (1999).

[41] J. Zaanen and O. Gunnarsson, Phys. Rev. B**40**, 7391 (1989).

[42] J.M. Tranquada, D.J. Buttery, and V. Sachan, Phys. Rev. B**54**, 12318 (1996).

[43] J.M. Tranquada, J.D. Axe, N. Ichikawa, A.R. Moodenbaugh, Y. Nakamura, and S. Uchida, Phys. Rev. Lett. **78**, 338 (1997).

[44] T. Suzuki, T. Goto, K. Chiba, T. Fukase, H. Kimura, K. Yamada, M. Ohashi, and Y. Yamaguchi, Phys. Rev. B**57**, 3229 (1998).

[45] K. Yamada, C.H. Lee, K. Kurahashi, J. Wada, S. Wakimoto, S. Ueki, H. Kimura, and Y. Endoh, Phys. Rev. B**57**, 6165 (1998).

[46] M. Arai, T. Nishijima, Y. Endoh, T. Egami, S. Tajima, K. Tomimoto, Y. Shiohara, M. Takahashi, A. Garrett, and S.M. Bennington, Phys. Rev. Lett. **83**, 608 (1999).

[47] S. Wakimoto, R.J. Birgeneau, M.A. Kastner, Y.S. Lee, R. Erwin, P.M. Gehring, S.H. Lee, M. Fujita, K. Yamada, Y. Endoh, K. Hirota, and G. Shirane, Phys. Rev. B**61**, 3699 (2000).

[48] M. Matsuda, M. Fujita, K. Yamada, R.J. Birgeneau, M.A. Kastner, H. Hiraka, Y. Endoh, S. Wakimoto, and G. Shirane, Phys. Rev. B**62**, 9148 (2000).

[49] H.A. Mook, D. Pengcheng, F. Dogan and R.D. Hunt, Nature **404**, 729 (2000).

[50] T. Yanagisawa, S. Koike and K. Yamaji, Physica B**284** (2000) 467; ibid. **281**, 933 (2000).

[51] T. Yanagisawa, S. Koike and K. Yamaji, J. Phys. Soc. Jpn. **68**, 3608 (1999).

[52] C. Gros, Ann. Phys. **189**, 53 (1989).

[53] T. Giamarchi and C. Lhuillier, Phys. Rev. B**43**, 12943 (1991).

[54] K. Yamaji, T. Yanagisawa and S. Koike, Physica B**284**-**288**, 415 (2000); Physica C**341**, 141 (2000).

[55] T. Yanagisawa, S. Koike and K. Yamaji, J. Phys. Soc. Jpn. **67**, 3867 (1998).

[56] C.J. Umrigar, K.G. Wilson, and J.W. Wilkins, Phys. Rev. Lett. **60**, 1719 (1988).

[57] P. Prelovsek, Phys. Lett. A**126**, 287 (1988).

[58] M. Inui and S. Doniach, Phys. Rev. B**38**, 6631 (1988).

[59] T. Yanagisawa, Phys. Rev. Lett. **68**, 1026 (1992); T. Yanagisawa and Y. Shimoi, Phys. Rev. B**48**, 6104 (1993).

[60] H. Eskes, G.A. Sawatzky, L.F. Feiner, Physica C**160**, 424 (1989).

[61] M.S. Hybertson, E.B. Stechel, M. Schlüter, D.R. Jennison, Phys. Rev. B**41**, 11068 (1990).

[62] A.K. McMahan, J.F. Annett, and R.M. Martin, Phys. Rev. B**42**, 6268 (1990).

[63] J.W. Loram, K.A. Mirza, J.R. Cooper, and W.Y. Liang, Phys. Rev. Lett. **71**, 1470 (1993).

[64] P.W. Anderson, Science **279**, 1196 (1998).

[65] Z. Hao, J.R. Clem, M.W. McElfresh, L. Civale, A.P. Malozemoff, and F. Holtzberg, Phys. Rev.B **43**, 2844 (1991).

[66] C.C. Tsuei and J.R. Kirtley, Phys. Rev. Lett. **85**, 182 (2000).

[67] T. Giamarchi and C. Lhuillier, Phys. Rev. B**42**, 10641 (1990).

[68] S. White and D.J. Scalapino, Phys. Rev. Lett: **80**, 1272 (1998).

[69] S. White and D.J. Scalapino, Phys. Rev. Lett: **81**, 3227 (1998).

[70] C.S. Hellberg and E. Manousakis, Phys. Rev. Lett: **83**, 132 (1999).

[71] K. Kobayashi and H. Yokoyama, J. Low Temp. Phys. **117**, 199 (1999).

[72] S. Kashiwaya, T. Ito, K. Oka, S. Ueno, H. Takashima, M. Koyanagi, Y. Tanaka and K. Kajimura, Physical Review B**57**, 8680 (1998).

[73] T. Nakano, N. Momono, M. Oda and M. Ido, J. Phys. Soc. Jpn. **67**, 2622 (1998).